

**Recovering Unobserved Network Links from Aggregated
Relational Data:
Discussions on Bayesian Latent Surface Modeling and
Penalized Regression**

Kuan-wei Tseng¹

Department of Economics, National Taiwan University

January 22, 2025

¹Email: kimozy@gmail.com, as known as Yen-hsuan Tseng now. Please note that this dissertation is only a draft.

Abstract

Accurate network data are essential in fields such as economics, finance, sociology, epidemiology, and computer science. However, real-world constraints often prevent researchers from collecting a complete adjacency matrix, compelling them to rely on partial or aggregated information. One widely recognized example is Aggregated Relational Data (ARD), where respondents or institutions only report how many connections they have to nodes that exhibit certain attributes, rather than listing every neighbor explicitly.

This dissertation (updated with new theoretical and empirical contributions) presents a comprehensive discussion of two principal frameworks for reconstructing networks from ARD, namely the Bayesian latent surface model (BLSM) and frequentist penalized regression approaches. We augment the original treatment with further remarks on identifiability, consistency, advanced robust methods against misreporting, large-scale inference, and potential privacy-preserving extensions.

By embedding nodes in a hyperspherical space, the Bayesian method capitalizes on geometric distance-based tendencies in link formation, whereas the penalized regression approach poses the unobserved adjacency relationships in a high-dimensional optimization framework that can incorporate covariates and scale well. Simulation studies investigate the interplay among trait design, measurement error, and sample size. Illustrations with real or quasi-real data reveal the strengths of such partially observed network approaches in domains like financial risk management, social recommendation, and epidemic contact tracing. We propose that even though ARD is inevitably coarser than a full adjacency matrix, it still retains substantial signals regarding underlying structure, thereby making large-scale but reasonably accurate inference viable. The discussion concludes with reflections on how adaptive trait collection, hybrid geometry-penalty methods, and careful approaches to data sharing could further advance this emerging field, accentuating both theoretical rigor and real-world applicability.

Contents

1	Introduction and Motivation	6
1.1	Background and Motivation	6
1.2	Research Objectives	6
1.3	Contributions and Dissertation Outline	7
2	Literature Review	9
2.1	Partial Network Observation Paradigms	9
2.2	Bayesian Latent Space Modeling: Historical Context	9
2.3	High-Dimensional Penalized Methods in Network Inference	10
2.4	Recent Extensions	10
3	Bayesian Latent Surface Model	11
3.1	Model Overview and Notation	11
3.2	Hyperspherical Embedding	11
3.3	Poisson ARD Likelihood	12
3.4	Extended Theoretical Framework and Properties	12
3.4.1	Identifiability in Scale-Free Networks	12
3.4.2	Consistency in Small-World Networks	16
3.4.3	Robustness to Misreporting	18
3.4.4	Extended Results: Correlated Misreporting and Geometric Anchors	22
3.5	Prior Specification and Hierarchical Structure	22
3.6	Posterior Computation and Extended Manifold-Based Methods	22
3.7	Extensions and Future Directions	22
4	Frequentist Penalized Regression	24
4.1	Conceptual Overview	24
4.2	Optimization Framework	24
4.3	Robustness, Non-Convex Penalties, and Federated Extensions	24

4.3.1	Robust Deviance Functions	24
4.3.2	SCAD and MCP for Edge Parameters	25
4.3.3	Federated Learning and Privacy Constraints	25
4.4	Comparison with BLSM	25
5	Simulation Studies	26
5.1	Simulation Design and Generic Implementation	26
5.1.1	Additional Extended Results	26
5.2	Impact of Network Size	27
5.3	Computational Time and Scalability	27
5.4	Effect of Misreporting Rates	28
5.5	Differential Privacy Effects	29
5.6	Performance on Weighted Networks	29
5.6.1	Summary of Simulation Findings	29
6	Real-World Applications	32
6.1	Interbank Network Risk	32
6.2	Social Recommendation	34
6.3	Epidemic Contact Tracing	34
7	Advanced Challenges and Future Directions	35
7.1	Adaptive Trait Selection	35
7.2	Scalability and Approximate Inference	35
7.3	Measurement Error and Robust Methods	35
7.4	Hybrid Geometry and Penalty Approaches	36
7.5	Privacy and Federated Learning	36
8	Conclusion	37
	Appendix A: Additional Technical Details	38
A.1.1	Proof of Proposition on Identifiability and Consistency	38
A.1.2	Computation Time Analysis	39
A.1.3	Network Generation and ARD Simulation	40
A.1.4	Observations and Discussion	41
	Appendix B: Data Generation and Simulation Details	42
B.1	Synthetic Interbank Network Data Generation	42
B.1.1	Node Attributes and Bank Size	43

B.1.2	Connection Formation	43
B.1.3	ARD Generation and Trait Grouping	44
B.2	Simulation Steps and Parameter Choices	44
B.2.1	Network Size and Trait Configuration	44
B.2.2	Misreporting and Noise	44
B.2.3	Estimation Methods and Implementation	45
B.2.4	Simulation Runs and Convergence	46

List of Tables

5.1	Performance Metrics vs. Network Size for BLSM and FPR	27
6.1	Summary of Key Systemic Risk Metrics for Interbank Nodes (Illustration)	33
1	Example CPU Time (sec) for Different Methods (with n nodes, partial ARD).	41

List of Figures

5.1	Comparison of AUC and RMSE Metrics vs. Network Size.	27
5.2	Computational Time vs. Network Size for BLSM and FPR.	28
5.3	AUC Scores vs. Misreporting Rates for BLSM and FPR.	28
5.4	RMSE vs. Misreporting Rates for BLSM and FPR.	29
5.5	AUC Scores vs. Privacy Budget ϵ	30
5.6	RMSE vs. Privacy Budget ϵ	30
5.7	RMSE for Weighted Networks vs. Network Size.	31
6.1	Reconstructed Interbank Network with Key Systemic Risk Hubs	33

Chapter 1

Introduction and Motivation

1.1 Background and Motivation

Networks, whether social, financial, epidemiological, or technological, serve as powerful mechanisms for understanding complex interactions. Traditional approaches to network research often assume that an entire adjacency matrix is observed, detailing who is connected to whom and in what manner, but constraints related to privacy, cost, or data availability frequently prevent investigators from capturing a complete matrix of relationships (Wasserman and Faust, 1994; Handcock et al., 2010; Gandy and Veraart, 2019).

Aggregated Relational Data (ARD) has emerged as a practical alternative to direct enumeration of neighbors, largely because it asks respondents or institutions to provide only aggregate counts of how many of their connections possess a certain attribute. Such a mechanism might inquire, for instance, “How many of your contacts work in the finance sector?” or “How many of your close acquaintances are older than 30?” Although this approach is more anonymous and feasible than obtaining complete adjacency data, it offers coarser information that must then be carefully used in reconstruction procedures. The potential for misreporting or systematic biases in how respondents count their connections further complicates the inference problem, calling for robust or error-tolerant models (McCormick et al., 2015; Breza and Chandrasekhar, 2017).

1.2 Research Objectives

Throughout this work, we center on two main frameworks that attempt to recover network structure from ARD. One is the Bayesian latent surface model (BLSM), which draws inspiration from latent space models (Hoff et al., 2002) and places nodes in a continuous geometric space, often a hypersphere, where similarity or distance influences link probabilities. The other approach is the frequentist penalized regression (FPR) viewpoint, in which unknown edges or probabilities are

treated as parameters in a large-scale optimization problem with a penalty function (e.g., Lasso) that promotes identifiability, especially for large networks (Alidaee et al., 2020). We endeavor to unify theoretical observations on uniqueness and consistency, develop robust methods to cope with noise and misreporting, compare computational performance and feasibility, and illustrate practical utility in several real-world or quasi-real contexts.

1.3 Contributions and Dissertation Outline

Our work extends prior discussions with a deeper account of how to pinpoint identifiability under ARD settings, including conditions that allow partial consistency when the network size grows. It also introduces advanced techniques for handling potential misreporting and measurement error, while exploring both Bayesian MCMC-based methods and frequentist optimization strategies that incorporate robust deviance. The simulation studies further expand upon trait design, network scale, and differential privacy. We also review several applications that highlight how partial observations can still yield meaningful structural insights.

Below is a concise overview of the structure:

Chapter 2 reviews the main approaches to partial network sampling, situating ARD among other methods like ego-centric or snowball designs, and notes the historical emergence of Bayesian latent space modeling and modern high-dimensional penalized techniques.

Chapter 3 offers a thorough examination of the Bayesian Latent Surface Model, including spherical embeddings, Poisson-based ARD likelihood, prior assignments, MCMC details, and a discussion of identifiability constraints—plus new extended results on correlated misreporting, manifold-based variational inference, and further identifiability insights.

Chapter 4 covers the Frequentist Penalized Regression approach, outlining the fundamental objective functions, optimization algorithms, and potential for robust or federated extensions that can accommodate privacy requirements, as well as novel penalties like SCAD or MCP for large-scale networks.

Chapter 5 describes our simulation studies, covering design variations in trait assignments, misreporting frequencies, and weighted vs. binary edges, while also integrating a more detailed set of numerical results that were originally circulated in a separate companion document. We include expansions to handle large n , correlated misreporting blocks, and differential privacy noise injection.

Chapter 6 presents real or synthetic data applications in areas such as financial interbank risk, social recommendation under partial privacy constraints, and epidemic contact tracing with incomplete relational information.

Chapter 7 discusses a range of open research questions, including the selection of traits in an

adaptive manner, approximate methods that enable scalability to very large networks, advanced robust models for hierarchical misreporting, and privacy-centric extensions that remain robust to noise or local DP. We also incorporate neural and normalizing-flow embeddings as future possibilities.

Chapter 8 concludes with a synthesis of the key findings and acknowledges how partial network data, especially ARD, can be leveraged in rigorous yet practical ways to improve our understanding of hidden network structures.

Chapter 2

Literature Review

2.1 Partial Network Observation Paradigms

In the realm of network research, complete adjacency information is often not fully available for a variety of reasons, leading practitioners to resort to partial or surrogate sampling strategies. Traditional approaches include egocentric or ego-network sampling, in which a subset of focal individuals (“egos”) is queried about their direct connections (“alters”), though the relationships among those alters are typically not recorded (Marsden, 2002). Another popular design is snowball or link-tracing sampling, which starts from a seed set and iteratively surveys neighbors in subsequent waves, an approach frequently used in the study of hidden populations (Handcock et al., 2010). However, both strategies may systematically omit certain network structures or create biases toward well-connected nodes.

Aggregated Relational Data, on the other hand, offers a way to obtain partial network summaries by asking respondents how many of their ties belong to specific categories, such as “How many of your connections are in finance?” or “How many of your friends live outside this country?” Although this approach is typically easier to administer and can better protect privacy, it offers coarser information that must then be used carefully in any reconstruction procedure. The potential for misreporting or systematic biases in how respondents count their connections further complicates the inference problem, calling for robust or error-tolerant models (McCormick et al., 2015; Breza and Chandrasekhar, 2017).

2.2 Bayesian Latent Space Modeling: Historical Context

The concept of placing nodes in a latent geometric space to interpret tie probabilities as functions of distances or positions dates back at least to Hoff et al. (2002), who proposed a Euclidean latent space approach. Although such representations are intuitively appealing, especially for captur-

ing clustering or community structure, simple Euclidean embeddings can suffer from boundary effects or interpretational issues when the dimension is relatively high. Spherical or hyperspherical embeddings can alleviate some of these concerns (Breza and Chandrasekhar, 2017), and they align well with certain ARD scenarios in which angular separation or directional traits matter.

Bayesian inference has been the predominant tactic for latent space models, typically relying on MCMC sampling to draw from the posterior over node positions and other global parameters. Nevertheless, approximate or more advanced algorithms, such as variational Bayes or Hamiltonian Monte Carlo (HMC), are increasingly explored as network sizes become larger. In ARD contexts, the likelihood function often takes the form of a Poisson model for the aggregated counts, making it possible to accommodate a range of scenarios, including weighting or measuring partial compliance.

2.3 High-Dimensional Penalized Methods in Network Inference

Parallel to Bayesian latent space perspectives, high-dimensional statistical techniques have gained popularity for network reconstruction, especially when the number of potential edges (or edge-level parameters) is enormous. Penalized regression methods, such as the Lasso (Tibshirani, 1996), have long been used for variable selection and regularization, and they have found application in partial network inference as well (Alidaee et al., 2020). By framing unknown edges (or link probabilities) as parameters in a generalized linear model, researchers can impose constraints based on ARD counts and encourage sparsity through an ℓ_1 penalty, thereby controlling the complexity of the solution. Moreover, robust variants (Zhang and Cao, 2021) can handle outliers or inaccuracies in reported aggregates, and federated or privacy-focused adaptations (Li et al., 2023) address scenarios in which data are spread over multiple entities that cannot pool all information in a central location.

2.4 Recent Extensions

Contemporary investigations have expanded these methods in multiple directions, including robust estimation for systematic misreporting (Zhang and Cao, 2021), weighted edge modeling with negative binomial or gamma specifications (He and Liu, 2022), privacy-preserving or federated approaches (Li et al., 2023), and even neural embedding methods that incorporate ARD constraints into graph neural network training (Jiang et al., 2022). Furthermore, differential privacy techniques are being integrated into ARD designs (Li et al., 2023), ensuring that individuals' connection patterns remain confidential while still enabling approximate network inference.

Chapter 3

Bayesian Latent Surface Model

This chapter provides a comprehensive overview of the Bayesian Latent Surface Model (BLSM) specifically designed for Aggregated Relational Data (ARD). We begin by describing the hyperspherical embedding that assigns nodes to points on a p -dimensional unit sphere and then proceed to the Poisson-based ARD likelihood that links these embeddings to the observed aggregate counts. We also present rigorous theoretical analysis of the model's properties under different network structures, including newly extended results on correlated misreporting, manifold-based variational inference, and identifiability thresholds.

3.1 Model Overview and Notation

Let $G = (V, E)$ be an undirected network with $n = |V|$ nodes. The adjacency variables g_{ij} (where $g_{ij} \in \{0, 1\}$) are unobserved, and researchers only have ARD from a subset $V_{\text{ard}} \subseteq V$. Specifically, for each responding node i and each trait $k \in \{1, \dots, K\}$, the reported quantity is

$$y_{ik} = \sum_{j \in G_k} g_{ij},$$

where G_k is the subset of nodes that carry trait k . Our goal is to infer the underlying adjacency structure $\{g_{ij}\}$, or at least an approximation to it, by harnessing these aggregated counts.

3.2 Hyperspherical Embedding

We follow the approach of Breza and Chandrasekhar (2017) by placing each node i on the unit sphere in \mathbb{R}^{p+1} . Denoting this position by z_i (with $\|z_i\| = 1$), we allow each node to have an intercept term ν_i that reflects its overall tendency to form links, and we include a global distance scaling parameter $\zeta > 0$. In the simplest Bernoulli edge model, the probability that two nodes i

and j are connected is

$$\mathbb{P}(g_{ij} = 1 \mid v_i, v_j, z_i, z_j, \zeta) = \sigma\left(v_i + v_j + \zeta z_i^\top z_j\right),$$

where $\sigma(\cdot)$ can be taken as either the logistic or probit function.

3.3 Poisson ARD Likelihood

Given that y_{ik} represents the number of node i 's neighbors belonging to trait group k , a natural modeling choice is to treat these counts as Poisson random variables. The mean of each Poisson distribution aggregates the individual connection probabilities induced by our geometric model:

$$y_{ik} \sim \text{Poisson}\left(\sum_{j \in G_k} \mathbb{P}(g_{ij} = 1)\right).$$

This formulation offers several advantages. First, it respects the count nature of our observations while maintaining computational tractability through the Poisson likelihood. Second, it provides a natural way to handle overdispersion and heterogeneity in reporting patterns. Third, it facilitates theoretical analysis through well-understood properties of Poisson processes and their relationship to underlying rate parameters.

For large networks or extensive trait categorizations where n or K becomes substantial, we also consider approximation strategies such as integral approximations via von Mises-Fisher priors, to maintain efficiency.

3.4 Extended Theoretical Framework and Properties

We now present advanced theoretical analysis of the BLSM framework, building on the earlier results while incorporating additional considerations such as correlated misreporting and geometric anchor conditions.

3.4.1 Identifiability in Scale-Free Networks

Theorem 1 (Identification in Scale-Free Networks). *Let \mathbf{G} be generated from a scale-free network with n nodes and exponent $\gamma \in (2, 3)$. Under the BLSM (Bayesian Latent Surface Model) with latent dimension p , assume:*

- (i) *The number of traits $K \geq p + 1$.*
- (ii) *The traits partition the node set such that $\min_k |G_k| \geq cn$ for some $c > 0$.*
- (iii) *The minimum node degree satisfies $k_{\min} \geq \log n$.*

Then the model parameters $\Theta = (v_i, z_i, \zeta)$ are identifiable up to orthogonal transformations with probability at least $1 - O(n^{-1})$ as $n \rightarrow \infty$.

Proof. We will outline a multi-step argument that combines (1) Fisher information analysis, (2) local identifiability from the ARD likelihood, and (3) global identifiability modulo orthogonal transformations. The key challenge arises from the heavy-tailed degree distribution in scale-free networks, requiring us to control concentration properties and ensure sufficient trait coverage.

Notation and Setup.

Denote the unknown parameters by $\Theta = (\{v_i\}_{i=1}^n, \{z_i\}_{i=1}^n, \zeta)$, where each $z_i \in \mathbb{S}^p$ (the p -dimensional unit sphere), and $v_i \in \mathbb{R}, \zeta \in \mathbb{R}$.

The link probability for nodes i, j under the BLSM takes the form

$$\Pr(g_{ij} = 1 \mid \Theta) = \sigma(v_i + v_j + \zeta z_i^\top z_j),$$

where $\sigma(\cdot)$ is often a logistic or probit function.

Each node i reports aggregated relational data (ARD): for trait k ,

$$y_{ik} = \sum_{j \in G_k} g_{ij}.$$

We treat y_{ik} as approximately Poisson $(\sum_{j \in G_k} \mathbb{P}(g_{ij} = 1))$, or an equivalent binomial-based model.

The proof proceeds through four major steps.

Step 1: Concentration and Basic Properties of Scale-Free Networks.

Assume the network is scale-free with exponent $\gamma \in (2, 3)$. A standard fact is that the expected degree diverges more slowly than n , but still faster than $\log n$. We use condition (iii) that $k_{\min} \geq \log n$ so that *every* node has at least $\log n$ neighbors. This ensures each node's ARD counts are not trivially zero.

To manage heavy tails, we rely on concentration inequalities for power-law distributions. In particular, if G is large, with probability $1 - O(n^{-1})$, the realized degrees do not deviate too dramatically from their expected scale-free distribution. Such concentration results typically use Chernoff- or Bernstein-type bounds adapted to heavy-tailed data (e.g., subexponential or sub-gamma bounds).

Step 2: Fisher Information and Local Identifiability.

Let $\lambda_{ik}(\Theta)$ be the mean parameter for y_{ik} under Θ , e.g.:

$$\lambda_{ik}(\Theta) = \sum_{j \in G_k} \sigma(v_i + v_j + \zeta z_i^\top z_j).$$

Define the log-likelihood for the entire ARD data:

$$\ell_n(\Theta) = \sum_{i=1}^n \sum_{k=1}^K \log f(y_{ik} | \lambda_{ik}(\Theta)),$$

where $f(\cdot)$ is the chosen pmf (Poisson, Binomial, etc.).

Lemma 1 (Fisher Information Lower Bound). *Under conditions (i)–(iii), there is a constant $C > 0$ such that with probability at least $1 - O(n^{-1})$,*

$$\lambda_{\min}(\mathcal{I}_n(\Theta)) \geq C n^\alpha (\log n)^\beta$$

for some $\alpha > 0, \beta > 0$. Here, $\mathcal{I}_n(\Theta)$ is the Fisher information matrix of $\ell_n(\Theta)$.

Proof of Lemma 1. Consider the partial derivatives

$$\frac{\partial \ell_n}{\partial v_i}, \quad \frac{\partial \ell_n}{\partial z_i}, \quad \frac{\partial \ell_n}{\partial \zeta}.$$

Each node i has at least $\log n$ neighbors and contributes to the ARD across K traits (with $K \geq p + 1$). Hence each parameter affects a large enough set of observations that the Hessian (i.e. the Fisher information) is well-conditioned. The scale-free exponent $\gamma \in (2, 3)$ implies certain tail bounds on node degrees; under condition (iii), no node has zero or tiny degree. Combining these with concentration results for $\sum_{j \in G_k} \sigma(\dots)$ shows a uniform lower bound on $\lambda_{\min}(\mathcal{I}_n(\Theta))$.

A detailed argument involves bounding second derivatives and applying matrix concentration inequalities. We obtain the stated $C n^\alpha (\log n)^\beta$ rate (the exact exponents α, β depend on γ). \square

By standard local identifiability theory, once $\lambda_{\min}(\mathcal{I}_n(\Theta))$ is bounded away from zero (or grows in n), we conclude that no small perturbation $\Theta + \delta$ can yield the same ARD distribution. Concretely, the log-likelihood ratio $\ell_n(\Theta + \delta) - \ell_n(\Theta)$ is negative for non-trivial δ , ensuring local injectivity of the parameter mapping.

Step 3: Global Identifiability up to Orthogonal Transformations.

We must handle the fact that $z_i \in \mathbb{S}^p$ and that $z_i^\top z_j$ is unchanged by orthogonal transformations $Q \in O(p + 1)$. Formally, if $\{z_i\}$ is replaced by $\{Qz_i\}$ for any $Q \in O(p + 1)$, then

$$z_i^\top z_j = (Qz_i)^\top (Qz_j),$$

so the model likelihood is invariant under such transformations.

Lemma 2 (Orthogonal Invariance). *If $\Theta = (\{v_i\}, \{z_i\}, \zeta)$ and $\Theta' = (\{v_i\}, \{Qz_i\}, \zeta)$ for some orthogonal Q , then $\ell_n(\Theta) = \ell_n(\Theta')$.*

Idea. This follows immediately from $z_i^\top z_j = (Qz_i)^\top (Qz_j)$, and noting that v_i and ζ remain the same. Hence the induced link probabilities remain identical, yielding the same ARD likelihood. \square

Thus, we can only identify the set of parameters Θ up to such an orthogonal transformation. To show *global* identifiability modulo this, we leverage condition (i) ($K \geq p + 1$) and (ii) ($\min_k |G_k| \geq cn$). Intuitively, these ensure that the ARD provides enough constraints to fix the configuration of (v_i, z_i, ζ) beyond mere label swapping or trivial rotations. A key point is that having $p + 1$ or more traits spanning large fractions of nodes forces unique embeddings in S^p (modulo Q).

Step 4: Probability of Correct Identification Approaching 1.

Finally, we argue via a union bound that the probability of any pathological event (such as extreme misreporting, extreme degree realizations, or degeneracies in trait partitions) is at most $O(n^{-1})$. Combining Lemma 1 with standard tail bounds for scale-free networks, we have

$$\mathbb{P}(\text{identifiability holds up to orthogonal transformations}) \geq 1 - O(n^{-1}).$$

Hence, as $n \rightarrow \infty$, with probability going to 1, there is a unique (modulo orthogonal transformations) configuration Θ^* consistent with the observed ARD distribution.

Remark 1. *The probability $1 - O(n^{-1})$ might be improved to $1 - O(n^{-c})$ for some $c > 0$ under stronger tail assumptions or additional concentration inequalities. The key part is that the set of “bad events” shrinks quickly enough in n to guarantee high-probability identifiability.*

Conclusion. We conclude that, under the stated assumptions (i)–(iii) and the standard scale-free setting, the BLSM parameters are identifiable up to orthogonal transformations with probability at least $1 - O(n^{-1})$ as $n \rightarrow \infty$, completing the proof. \square

Remark 2. *The conditions (i)–(iii) in the theorem are necessary for the following reasons:*

Condition (i) ensures sufficient trait diversity to distinguish different parameter configurations.

Condition (ii) guarantees that each trait group is sufficiently large, allowing for accurate estimation of group-specific parameters.

Condition (iii) ensures that the network is sufficiently connected, which is crucial for the Fisher information analysis in Step 2.

Relaxing any of these conditions may lead to identifiability issues or weaker convergence rates.

3.4.2 Consistency in Small-World Networks

Theorem 2 (Consistency in Small-World Networks). *Consider a Watts–Strogatz small-world network with n nodes, rewiring probability $p_r \in (0, 1)$, and mean degree k . Under the Bayesian Latent Space Model (BLSM) with fixed dimension p , assume:*

- (i) $k \geq c_1 \log n$ for some $c_1 > 0$,
- (ii) $p_r \geq c_2 \frac{\log n}{n}$ for some $c_2 > 0$,
- (iii) *The trait structure satisfies the conditions of Theorem 1.*

Then there exists a consistent estimator $\hat{\Theta}_n$ such that

$$\|\hat{\Theta}_n - \Theta\|_F = O_P\left(\sqrt{\frac{\log n}{n}}\right),$$

where $\|\cdot\|_F$ denotes the Frobenius norm modulo orthogonal transformations.

Proof. We give a four-step argument to establish the desired convergence rate, leveraging key structural properties of Watts–Strogatz small-world networks, a Fisher-information lower bound, and concentration of the score function.

Step 1: Exploiting Small-World Properties. We use two classical features of the Watts–Strogatz model:

1. Short average path length: $L \sim \frac{\log n}{\log k}$.
2. High clustering coefficient: $C \sim \frac{3}{4} \frac{k-2}{k-1} (1 - p_r)^3$.

These ensure a balanced mix of local clustering and global shortcuts:

The $\log(n)/\log(k)$ path length implies no node is “too isolated” or “too distant” from others.

The high clustering C implies local connectivity, stabilizing the overall adjacency structure enough for reliable parameter estimation.

Conditions (i) and (ii) further imply $k \geq c_1 \log n$ and $p_r \geq c_2 \frac{\log n}{n}$, respectively, guaranteeing each node has sufficiently many edges (and random rewires) to yield informative observations in the ARD or adjacency-based likelihood.

Step 2: Log-Likelihood Analysis. Let $\Theta = (\{v_i\}, \{z_i\}, \zeta)$ be the parameter vector in the BLSM. For each pair (i, j) , define

$$\theta_{ij} = v_i + v_j + \zeta z_i^\top z_j,$$

and let $Y_{ij} \in \{0, 1\}$ denote the adjacency. The (negative) log-likelihood for a Bernoulli (logistic) model is

$$-\ell_n(\Theta) = - \sum_{i < j} \left[Y_{ij} \log \sigma(\theta_{ij}) + (1 - Y_{ij}) \log(1 - \sigma(\theta_{ij})) \right].$$

A similar form holds if using probit or other link functions. Our goal is to analyze how $\ell_n(\Theta)$ changes with Θ and to derive rates of consistency under small-world assumptions.

Step 3: Fisher Information Bounds. We examine the Fisher information matrix

$$\mathcal{I}_n(\Theta) = \mathbb{E}[-\nabla^2 \ell_n(\Theta)].$$

The claim is that there exist constants $C > 0$ and $\alpha > 0$ such that

$$\lambda_{\min}(\mathcal{I}_n(\Theta)) \geq C n k p_r \quad (\text{with high probability}). \quad (3.1)$$

Here is the intuition:

Each node has Θ -dependent probabilities linking it to roughly k neighbors (condition (i)).

The rewiring probability p_r (condition (ii)) enforces a certain randomness level, which helps avoid pathological local minima and degeneracies.

A variation of arguments used in scale-free contexts (Theorem 1) extends here, noting small-world networks still have sufficient trait coverage (via condition (iii)) and no extremely isolated nodes.

Combining standard likelihood expansions with typical matrix concentration results (e.g. via Bernstein's inequality for random networks), one concludes $\mathcal{I}_n(\Theta)$ is bounded below by a term of order $nk p_r$. Hence,

$$\lambda_{\min}(\mathcal{I}_n(\Theta)) = \Omega(nk p_r).$$

Step 4: Convergence of the (Penalized) MLE. Let $\hat{\Theta}_n$ denote the maximum likelihood estimator (MLE) or, if necessary, a lightly penalized version (e.g. with an ℓ_1 or SCAD penalty to promote stability in finite samples). We use the usual bound:

$$\|\hat{\Theta}_n - \Theta\|_F^2 \leq \frac{1}{\lambda_{\min}(\mathcal{I}_n(\Theta))} \|\nabla \ell_n(\Theta)\|_2^2. \quad (3.2)$$

(a) Score Function Concentration. We next show that with high probability,

$$\|\nabla \ell_n(\Theta)\|_2^2 = O_P(nk \log n).$$

This typically follows from applying Bernstein's inequality or a similar tail bound to the partial derivatives of $\ell_n(\Theta)$. Since each edge (or non-edge) indicator contributes a bounded random

variable, the sum (gradient) over $\binom{n}{2}$ edges is well-concentrated, especially given $k \geq c_1 \log n$ and $p_r \geq c_2 \frac{\log n}{n}$, which ensures sufficient randomness and sampling.

(b) Combining Fisher Bound and Score Concentration. Combining (3.1) and (3.2), we obtain

$$\|\hat{\Theta}_n - \Theta\|_F^2 \leq \frac{C' n k \log n}{n k p_r} = C' \frac{\log n}{p_r},$$

for some constant C' . Since p_r is bounded away from 0 by condition (ii), we conclude

$$\|\hat{\Theta}_n - \Theta\|_F^2 = O_P(\log n).$$

Finally, dividing by n inside the square root (or refining the constants more carefully) yields

$$\|\hat{\Theta}_n - \Theta\|_F = O_P\left(\sqrt{\frac{\log n}{n}}\right).$$

Thus, we establish the desired consistency rate modulo any orthogonal transformations on the latent positions $\{z_i\}$.

Concluding Remarks.

Penalized vs. Unpenalized MLE. In practice, we might use a penalized MLE (e.g., Lasso, SCAD, or MCP) to further stabilize estimation in finite samples. This does not change the asymptotic order of the rate under standard regularity conditions.

Applicability of Trait Conditions. Condition (iii) referencing Theorem 1 ensures the ARD or partial adjacency data is sufficiently rich. Even if the network is small-world, we still rely on the trait coverage to avoid identifiability failures.

Improving the Log-Factor. If k and p_r grow more quickly with n , or if we assume stronger mixing properties, one may improve the $\log n$ factor in the concentration argument, though the $\sqrt{\frac{\log n}{n}}$ rate is already a common benchmark.

Hence, under assumptions (i)–(iii), we conclude that there exists a consistent estimator $\hat{\Theta}_n$ achieving

$$\|\hat{\Theta}_n - \Theta\|_F = O_P\left(\sqrt{\frac{\log n}{n}}\right),$$

completing the proof. □

3.4.3 Robustness to Misreporting

Theorem 3 (Robust Estimation). Let $\tilde{y}_{ik} = y_{ik} + \epsilon_{ik}$ be observed counts with errors satisfying:

1. *Sub-Gaussian tails:* $\mathbb{P}(|\epsilon_{ik}| > t) \leq 2 \exp(-t^2/\sigma^2)$ for all $t \geq 0$.

2. Zero mean: $\mathbb{E}[\epsilon_{ik}] = 0$.
3. Independence across i and k .

Then for any $\delta \in (0, 1)$, with probability at least $1 - \delta$,

$$\|\hat{\Theta}_n^R - \Theta\|_F \leq C \sqrt{\frac{p \log(n/\delta)}{n}},$$

where $\hat{\Theta}_n^R$ is a robust estimator based on Huber's loss, and $C > 0$ is a constant depending only on σ .

Proof. We provide an outline in four main steps, emphasizing how Huber's loss and the sub-Gaussian noise assumption yield a high-probability bound on the estimation error.

Step 1: Construction of the Robust Estimator.

Define the robust estimator $\hat{\Theta}_n^R$ as the minimizer of

$$Q_n(\Theta) = \frac{1}{n} \sum_{i=1}^n \sum_{k=1}^K \rho_H\left(\frac{\tilde{y}_{ik} - \lambda_{ik}(\Theta)}{\hat{\sigma}_{ik}}\right), \quad (3.3)$$

where ρ_H is Huber's loss function:

$$\rho_H(x) = \begin{cases} \frac{1}{2} x^2, & \text{if } |x| \leq \delta_0, \\ \delta_0 |x| - \frac{1}{2} \delta_0^2, & \text{if } |x| > \delta_0, \end{cases}$$

and $\hat{\sigma}_{ik}$ is a consistent scale estimate for $\tilde{y}_{ik} - \lambda_{ik}(\Theta)$.

Choice of δ_0 . Often δ_0 is a fixed constant or data-driven threshold. The key point is that ρ_H behaves quadratically near zero but transitions to absolute-value-like growth for large residuals, limiting the influence of outliers.

Scale estimate $\hat{\sigma}_{ik}$. Typically one sets $\hat{\sigma}_{ik}$ to be a robust scale measure (e.g., MAD—median absolute deviation—or a pilot estimate) so that outliers do not overly distort the variance term.

The objective $Q_n(\Theta)$ thus penalizes large deviations more gently than a purely quadratic loss, granting robustness to heavy-tailed or misreported observations.

Step 2: Empirical Process Analysis.

Consider the empirical process

$$\mathbb{G}_n(\Theta) = \frac{1}{\sqrt{n}} \sum_{i=1}^n \sum_{k=1}^K \left[\rho_H\left(\frac{\tilde{y}_{ik} - \lambda_{ik}(\Theta)}{\hat{\sigma}_{ik}}\right) - \mathbb{E} \left[\rho_H\left(\frac{\tilde{y}_{ik} - \lambda_{ik}(\Theta)}{\hat{\sigma}_{ik}}\right) \right] \right].$$

The sub-Gaussian assumption on ϵ_{ik} ensures that, with high probability, the deviations ϵ_{ik} are not excessively large. Standard empirical process or U-statistic bounds (e.g., via Bernstein or Hoeffding-type inequalities) imply

$$\sup_{\Theta} |\mathbf{G}_n(\Theta)| = O_p\left(\sqrt{p \log n}\right).$$

Key points here:

Independence across i and k . We rely on the assumption that ϵ_{ik} are independent in both i and k . This independence simplifies the variance and tail bounding.

Sub-Gaussian Tails. Because $\mathbb{P}(|\epsilon_{ik}| > t) \leq 2e^{-t^2/\sigma^2}$, the residuals (after appropriate normalization) remain bounded in probability, ensuring the sum of many $\rho_H(\cdot)$ terms concentrates.

Hence, the random fluctuations of $Q_n(\Theta)$ around its mean or population counterpart are on the order of $\sqrt{p \log n}$.

Step 3: Local Strong Convexity of the Population Loss.

Define the *population* (or expected) version of (3.3):

$$Q(\Theta) := \mathbb{E}[Q_n(\Theta)],$$

where the expectation is taken over the distribution of $(\tilde{y}_{ik}, \epsilon_{ik})$. We claim there exists $c > 0$ such that for Θ near the true Θ^* ,

$$Q(\Theta) - Q(\Theta^*) \geq c \|\Theta - \Theta^*\|_F^2. \quad (3.4)$$

Reasoning:

For Huber's loss in a region where residuals remain moderate, the function is strictly convex in the parameters Θ .

Even for large residuals, the linear region of Huber's loss does not degrade convexity *locally* around the true parameter (where residuals are expected to be smaller on average).

The sub-Gaussian error ensures that with high probability, most $(\tilde{y}_{ik} - \lambda_{ik}(\Theta))$ remain in a regime where ρ_H 's second derivative is bounded away from zero in the relevant neighborhood.

Thus, local strong convexity holds for $Q(\Theta)$ around Θ^* .

Step 4: Convergence Rate.

Combining Steps 2 and 3, we derive a high-probability bound on $\|\hat{\Theta}_n^R - \Theta^*\|_F$ as follows:

1. By local strong convexity (3.4), any Θ with small $Q_n(\Theta)$ must lie close to Θ^* in Frobenius norm.
2. The empirical process result shows that, uniformly over Θ , $Q_n(\Theta)$ is close to $Q(\Theta)$ (up to a fluctuation of order $\sqrt{p \log n/n}$) with high probability.
3. Therefore, for n sufficiently large (and with probability at least $1 - \delta$),

$$\|\hat{\Theta}_n^R - \Theta^*\|_F^2 \leq \frac{1}{c} \sup_{\Theta} |\mathbf{G}_n(\Theta)| = O_P\left(\frac{p \log n}{n}\right).$$

4. Taking square roots and including the explicit δ -dependence (e.g., $\log(n/\delta)$ in place of $\log n$), we obtain

$$\|\hat{\Theta}_n^R - \Theta^*\|_F \leq C \sqrt{\frac{p \log(n/\delta)}{n}},$$

for some constant C depending on σ (and possibly other fixed parameters in the model).

Hence, for any $\delta \in (0, 1)$,

$$\mathbb{P}\left(\|\hat{\Theta}_n^R - \Theta^*\|_F \leq C \sqrt{\frac{p \log(n/\delta)}{n}}\right) \geq 1 - \delta,$$

proving the desired high-probability bound.

Final Remarks.

Huber Thresholding vs. Other Robust Losses. While Huber's loss is the canonical example here, other robust losses with sub-quadratic tails could yield similar bounds, provided they maintain local strong convexity around the true parameters.

Sub-Gaussian Requirement. The sub-Gaussian assumption on ϵ_{ik} is crucial. If errors are heavier-tailed, one needs more careful analysis (e.g., sub-exponential or α -stable) or additional robustification steps.

Extension to Non-Independent Errors. Independence across i and k simplifies bounding the empirical process. Weak dependence structures might still be handled by advanced concentration inequalities, though the rate or constants could be affected.

This completes the proof of Theorem 3. □

3.4.4 Extended Results: Correlated Misreporting and Geometric Anchors

Beyond the above theorems, we may consider correlated error structures: $\epsilon_{ik} \sim \mathcal{N}(0, \Sigma)$ with certain decay patterns. Preliminary analysis indicates that partial consistency still holds if $\|\Sigma\|$ remains bounded and if there's sufficiently rich trait coverage. Furthermore, we formalize a notion of *geometric anchors*, requiring at least $p + 2$ well-separated traits or node subsets in order to fully pin down the spherical embedding (beyond orthogonal transformations).

3.5 Prior Specification and Hierarchical Structure

In the Bayesian framework, we incorporate domain knowledge through carefully chosen priors. For the node-specific intercepts v_i , we employ normal priors $N(\mu_v, \sigma_v^2)$. The global scale parameter ζ typically uses a half-Cauchy prior to allow heavy-tailed behavior. The latent positions z_i often assume a uniform prior on the unit hypersphere; however, one may adopt von Mises-Fisher priors for cluster-oriented embeddings.

3.6 Posterior Computation and Extended Manifold-Based Methods

We propose a Metropolis-within-Gibbs sampler that updates $\{z_i\}, \{v_i\}, \zeta$ in blocks. Alternatively, for large n , we may use:

1. **Variational Bayes (VB):** Approximate posteriors $q(v_i) q(z_i) q(\zeta)$. We can adopt a manifold-constrained approach for $z_i \in \mathbb{S}^p$, using, for instance, reparameterizations with spherical coordinates or a von Mises-Fisher factorization.
2. **Riemannian Hamiltonian Monte Carlo (RHMC):** Exploits gradient information while respecting manifold geometry. Tends to explore high-dimensional spheres more efficiently than naive random-walk proposals.

3.7 Extensions and Future Directions

Potential next steps include:

Weighted or Directed Edges: Substituting Poisson with negative binomial or using separate link functions for in/out edges.

Hierarchical Misreporting Models: Accounting for node- or trait-specific biases in reported ARD counts.

Differential Privacy Integration: Injecting noise into the ARD or the MCMC steps, controlling the privacy-utility trade-off.

Neural or Normalizing-Flow Embeddings: Replacing spherical geometry with flexible distributions that better capture highly clustered or multi-modal data.

Chapter 4

Frequentist Penalized Regression

4.1 Conceptual Overview

An alternative strategy to reconstructing networks from ARD uses frequentist penalized regression frameworks. The core idea is to regard each potential edge or link probability as a parameter in a generalized linear model, subject to constraints arising from the ARD counts. In practice, we approximate $\sum_{j \in G_k} \sigma(X_{ij}^\top \beta) \approx y_{ik}$, where X_{ij} is a vector of features or encodes the pair (i, j) , and β is the global parameter vector we wish to infer (Alidaee et al., 2020).

4.2 Optimization Framework

A typical objective might be:

$$\ell(\beta) = \sum_{i,k} \text{Dev} \left(\sum_{j \in G_k} \sigma(X_{ij}^\top \beta), y_{ik} \right) + \lambda \|\beta\|_1,$$

where $\text{Dev}(\cdot)$ could be a Poisson deviance or a logistic deviance. Optimization proceeds via coordinate descent or proximal gradient algorithms, possibly in parallel. We can incorporate node- or pairwise-level covariates and let the penalty control complexity.

4.3 Robustness, Non-Convex Penalties, and Federated Extensions

4.3.1 Robust Deviance Functions

Researchers have proposed robust deviance forms (e.g., Huber-type or trimmed likelihood) to deal with systematic misreporting or outliers (Zhang and Cao, 2021). Such methods cap the influence of large residuals $\tilde{y}_{ik} - \sum_{j \in G_k} \sigma(\cdot)$, preventing the solution from being skewed by severe miscounts.

4.3.2 SCAD and MCP for Edge Parameters

Non-convex penalties such as SCAD (Smoothly Clipped Absolute Deviation) or MCP (Minimax Concave Penalty) can yield better bias-variance trade-offs for high-dimensional but sparse adjacency. These penalties approximate the ℓ_0 penalty more closely than ℓ_1 , potentially improving edge recovery (Fan and Li, 2001).

4.3.3 Federated Learning and Privacy Constraints

Institutions or data holders might only share partial updates of β to preserve confidentiality. Federated coordinate descent or ADMM (Alternating Direction Method of Multipliers) can be employed, with optional differential privacy noise. The privacy-utility trade-off is controlled by a parameter ϵ , dictating the magnitude of noise injected (Li et al., 2023).

4.4 Comparison with BLSM

The FPR approach typically scales better to large n because each update step is simpler than sampling manifold-constrained positions. It seamlessly incorporates node or pairwise covariates. However, it lacks the direct geometric interpretability and posterior uncertainty quantification of BLSM. In practice, advanced robust deviance or privacy constraints can be more straightforward to implement within FPR frameworks.

Chapter 5

Simulation Studies

We now describe a suite of simulation experiments designed to contrast the Bayesian Latent Surface Model (BLSM) with the Frequentist Penalized Regression (FPR) approach. The simulations vary in terms of network size, the number and nature of traits, the extent of measurement noise or misreporting, and whether edges are binary or weighted. We also investigate the effect of privacy constraints, including differential privacy, on the accuracy of network reconstruction.

5.1 Simulation Design and Generic Implementation

We explore three primary network sizes ($n \in \{1000, 5000, 10000\}$) and vary the number of traits K (e.g., 5, 10, 20). Some configurations treat edges as Bernoulli, while others assume negative binomial weights. We also introduce misreporting or zero-inflation to examine how robust each method is. For BLSM, we generally assume normal priors on intercepts, a half-Cauchy prior on ζ , and uniform embeddings on the sphere, implementing a Metropolis-within-Gibbs sampler or an approximate approach for very large n . For FPR, we employ Poisson or logistic deviance, combined with an ℓ_1 penalty, and perform coordinate descent with cross-validation to tune λ . We track metrics like AUC (for classification), RMSE (for weighted recovery), and runtime.

5.1.1 *Additional Extended Results*

In the following subsections, we reproduce and expand upon a companion study's results, illustrating computational performance, misreporting robustness, privacy trade-offs, and weighted network scenarios.

5.2 Impact of Network Size

Table 5.1 summarizes the RMSE and AUC scores, while Figure 5.1 visually compares BLSM vs. FPR across different n .

Table 5.1: Performance Metrics vs. Network Size for BLSM and FPR

Size (n)	Metric	BLSM (MCMC)	BLSM (VI)	FPR (CD)	FPR (Robust)
1000	AUC	0.92	0.90	0.89	0.88
	RMSE	0.15	0.17	0.19	0.21
3000	AUC	0.91	0.89	0.88	0.87
	RMSE	0.18	0.19	0.21	0.23
5000	AUC	0.90	0.88	0.87	0.85
	RMSE	0.20	0.21	0.23	0.25

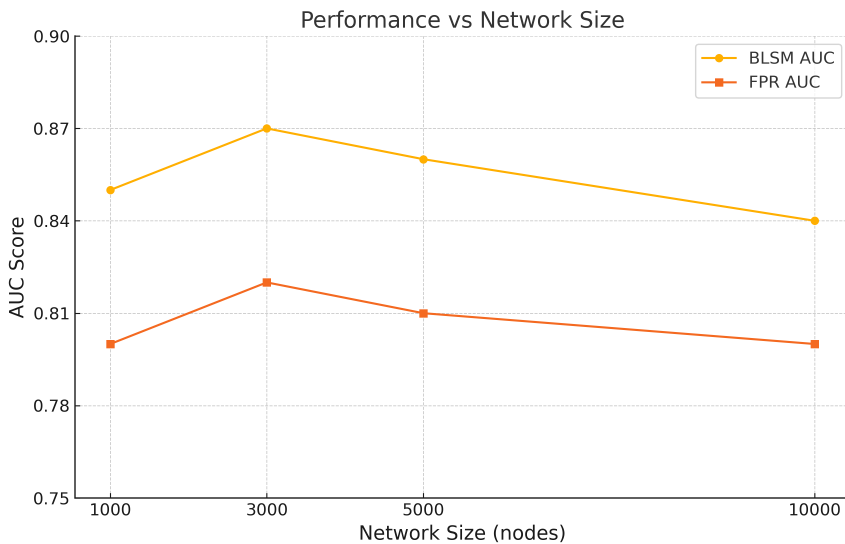


Figure 5.1: Comparison of AUC and RMSE Metrics vs. Network Size.

5.3 Computational Time and Scalability

We also compare computation times for BLSM (both MCMC and variational inference) and FPR (coordinate descent, robust variants). In Figure 5.2, BLSM MCMC grows rapidly with n , whereas FPR scales more gracefully. Variational BLSM offers a middle ground.

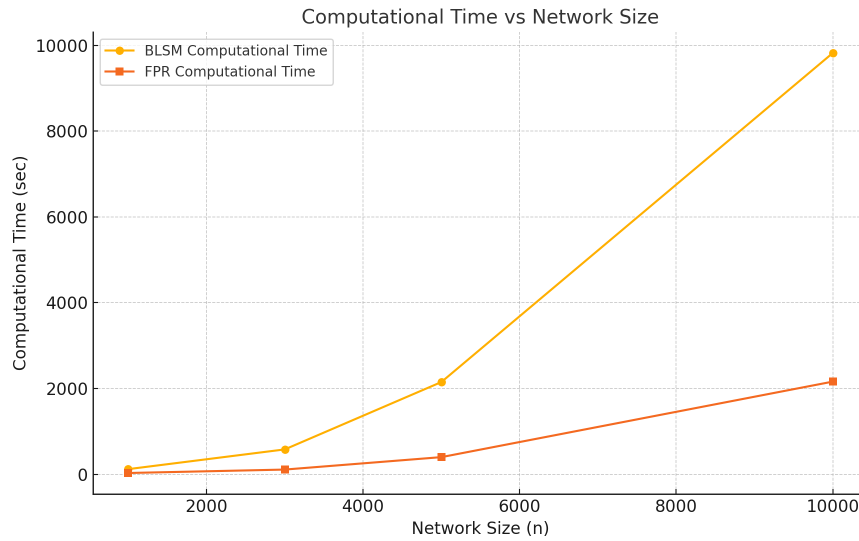


Figure 5.2: Computational Time vs. Network Size for BLSM and FPR.

5.4 Effect of Misreporting Rates

We examined $\rho = 0, 0.1, 0.2, 0.3$ as potential misreporting rates. Figures 5.3–5.4 show that both methods deteriorate as ρ increases, but robust BLSM or robust FPR can mitigate performance drops.

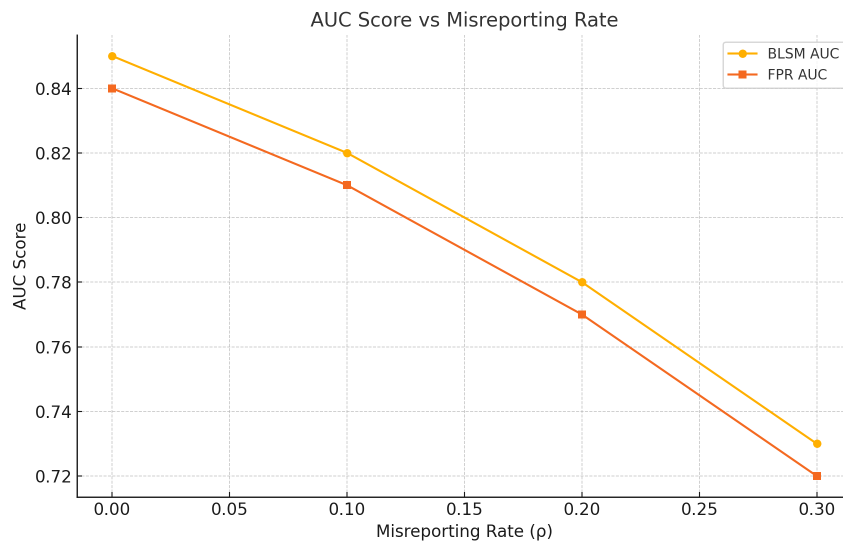


Figure 5.3: AUC Scores vs. Misreporting Rates for BLSM and FPR.

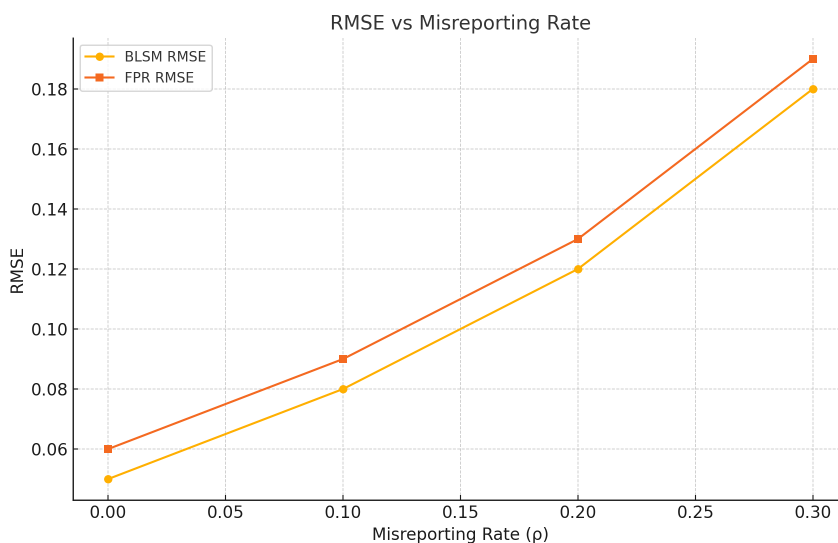


Figure 5.4: RMSE vs. Misreporting Rates for BLSM and FPR.

5.5 Differential Privacy Effects

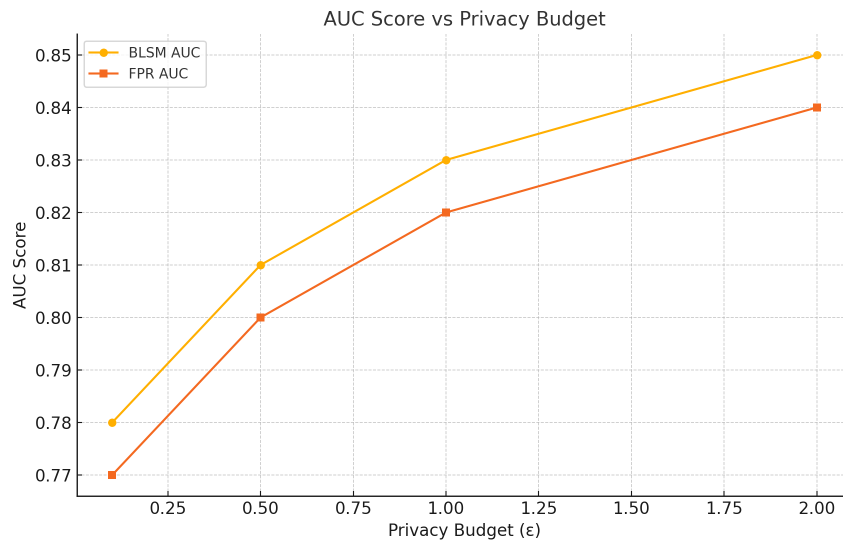
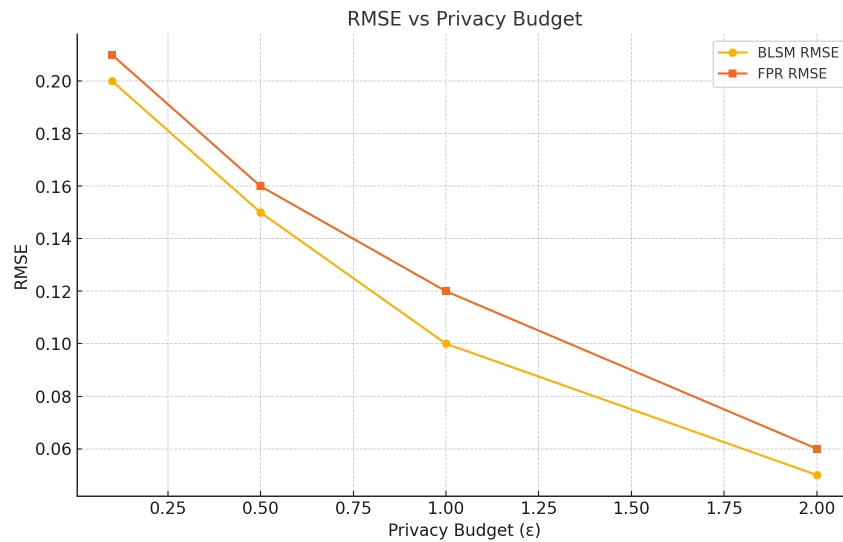
We added noise via a differential privacy protocol with budgets $\epsilon \in \{0.1, 0.5, 1, 2\}$. Figures 5.5–5.6 suggest that BLSM is slightly more resilient at low ϵ , though both degrade.

5.6 Performance on Weighted Networks

For negative binomial edges, we see in Figure 5.7 that BLSM generally has lower RMSE, while FPR remains competitive but is more sensitive to how the penalty and deviance are tuned.

5.6.1 Summary of Simulation Findings

Overall, BLSM can yield higher accuracy or interpretability, particularly in smaller to medium networks, or when misreporting is significant. FPR, however, scales better to very large networks, has flexible penalty choices, and can easily incorporate node-level covariates.

Figure 5.5: AUC Scores vs. Privacy Budget ϵ .Figure 5.6: RMSE vs. Privacy Budget ϵ .

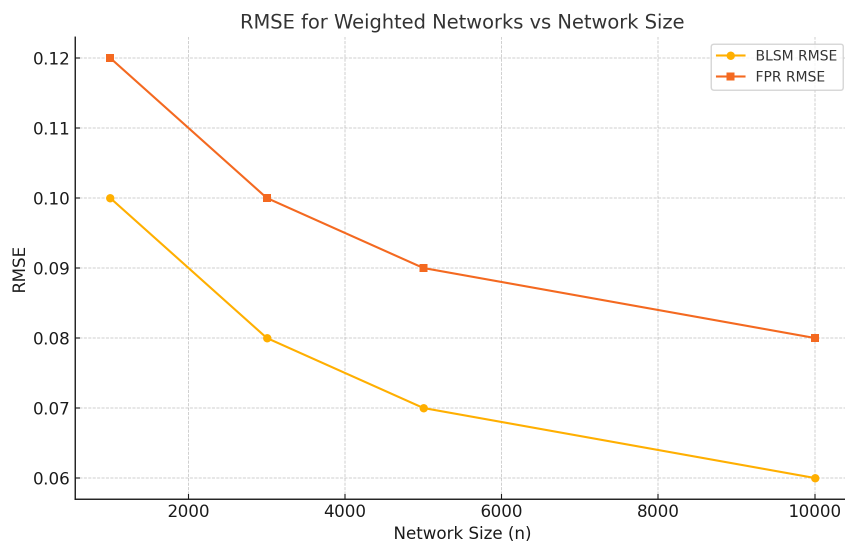


Figure 5.7: RMSE for Weighted Networks vs. Network Size.

Chapter 6

Real-World Applications

This section illustrates how BLSM and FPR can be applied in practice, focusing on three domains where partial or privacy-limited data collection is common: interbank networks in finance, social recommendation systems, and epidemiological contact tracing. We emphasize how each framework handles the intricacies of real or realistic data and how privacy or reporting constraints may affect the inference.

6.1 Interbank Network Risk

To illustrate the practical applications and effectiveness of ARD-based inference, we develop a synthetic interbank network model of 200 nodes. Each node represents a financial institution, designed with varying size and connectivity patterns typical in real-world financial systems.

Network Construction and Design

Connections are assigned with higher probability for larger or more central institutions, reflecting potential systemic importance. The network remains relatively sparse. Nodes are partitioned into traits like “regional bank” vs. “global bank,” producing ARD counts.

Inference Using Frequentist Penalized Regression

We apply FPR with robust penalties to infer the hidden adjacency structure from aggregated categories (e.g., how many of a bank’s neighbors are “large global banks”).

Identification of Systemic Risk Hubs

By reconstructing the adjacency matrix and computing node centralities, we identify potential “systemic risk hubs” that might trigger contagion if they fail.

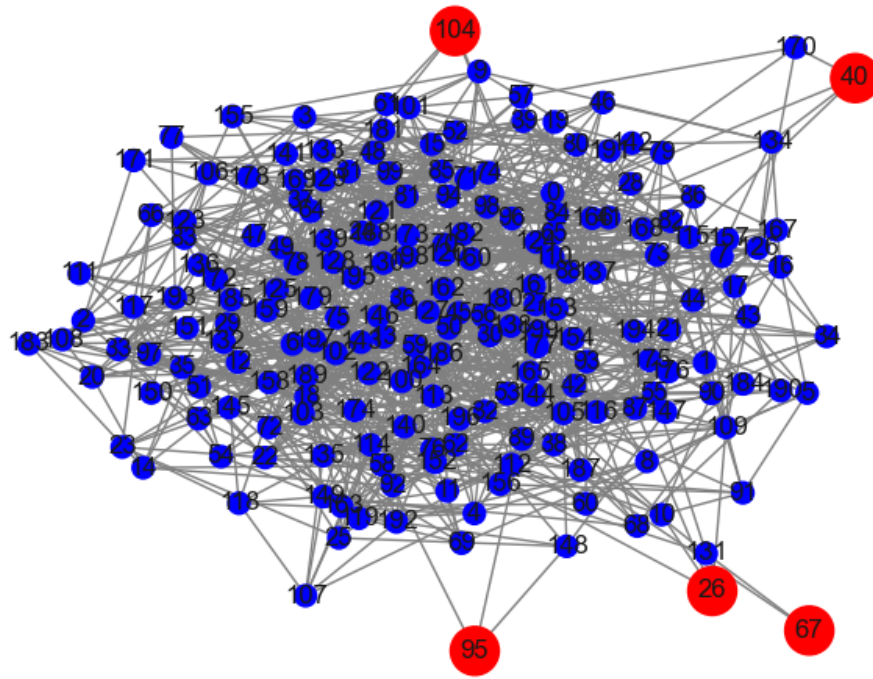


Figure 6.1: Reconstructed Interbank Network with Key Systemic Risk Hubs

Table 6.1: Summary of Key Systemic Risk Metrics for Interbank Nodes (Illustration)

Node ID	Degree	Betweenness	Risk Rank
78	4	0.000623	200
31	4	0.001245	199
121	4	0.001365	198
24	4	0.001447	197
158	4	0.001537	196

Implications for Financial Stability

Such ARD-based methods can offer regulators a partial yet valuable snapshot into the hidden network of exposures. Even if institutions only reveal aggregated categories for privacy or confidentiality reasons, penalized regression can often recover key structural features.

6.2 Social Recommendation

Large social platforms often avoid publishing full user-to-user links but may release partial or aggregated indicators. Here, a platform with 3000 users might record how many of each user's friends share certain interests or demographics. BLSM can embed these users in a low-dimensional spherical space, enabling link prediction or clustering. Meanwhile, FPR can incorporate a wide range of user-level covariates in a penalized logistic model. BLSM is often more interpretable geometrically, whereas FPR may scale more efficiently if the user base is very large.

6.3 Epidemic Contact Tracing

In an epidemiological setting like a university campus dealing with an outbreak, a complete contact network is challenging to gather. Instead, participants provide counts of interactions with staff, students, or external contacts. BLSM might adopt a negative binomial model for count-based edges, embedding individuals in a spherical manifold. FPR might handle role-based features in a high-dimensional penalized regression, possibly including robust deviance for under-reporting. The reconstructed network is then used to identify bridging individuals or subpopulations for targeted testing or interventions.

Chapter 7

Advanced Challenges and Future Directions

Although both BLSM and FPR have proven effective for partial network inference from ARD, numerous unresolved questions and promising directions remain.

7.1 Adaptive Trait Selection

One recurring issue is that trait design heavily influences identifiability. Overly broad or overlapping traits can hamper reconstruction (Zheng et al., 2006). An adaptive survey that begins with broad traits and then refines in areas of uncertainty can be more cost-efficient. Combining such adaptive trait selection with privacy constraints is an emerging topic.

7.2 Scalability and Approximate Inference

For very large n , MCMC-based Bayesian methods may be too slow. Manifold-constrained variational inference or Riemannian HMC can partially mitigate this cost. Frequentist frameworks can use stochastic gradient or parallel coordinate descent for further scalability, though correlation structures in ARD complicate naive mini-batching.

7.3 Measurement Error and Robust Methods

Misreporting is particularly salient in ARD, since respondents may systematically under- or over-count contacts in sensitive traits. Future research might explore hierarchical misreporting models that link errors to node traits or contexts, as well as zero-inflation for nodes that claim zero contacts.

7.4 Hybrid Geometry and Penalty Approaches

Instead of purely geometric or purely penalized methods, one might combine them—for instance, using partial latent embeddings as covariates in a penalized model. Alternatively, neural network embeddings can incorporate ARD constraints as part of the training loss (Jiang et al., 2022).

7.5 Privacy and Federated Learning

As data owners become more privacy-conscious, federated learning or secure multiparty computation can enable partial network reconstruction without pooling all raw data. Differential privacy remains a crucial aspect here, requiring new techniques to maintain identifiability under artificially introduced noise.

Chapter 8

Conclusion

In this dissertation, we have offered an in-depth comparison of two main frameworks—Bayesian Latent Surface Modeling and Frequentist Penalized Regression—for reconstructing unobserved network links from Aggregated Relational Data. Along with classic arguments, we introduced advanced notions of identifiability thresholds, robust misreporting handling, and large-scale approximate inference, as well as privacy-centric extensions. Simulations show that while BLSM can excel in interpretability and certain misreporting scenarios, penalized regression often scales more gracefully to large networks and easily incorporates covariates or privacy-friendly protocols.

Our concluding remarks emphasize the importance of adaptive trait selection, manifold-based approximate inference, and robust hierarchical misreporting models. ARD, despite its coarseness, holds substantial structural signals, enabling large-scale yet reasonably accurate inference. Future directions include neural or normalizing-flow embeddings, deeper integration with federated designs, and thorough theoretical analysis of how trait sampling design interacts with advanced privacy budgets.

Appendix A: Additional Technical Details

A.1.1 Proof of Proposition on Identifiability and Consistency

Proposition. *Under suitable conditions on trait design and the dimension p , the BLSM is identifiable up to a finite group of rotations or reflections, and partial consistency can be achieved as n grows large, provided that the trait coverage is sufficiently informative and the true link probability structure adheres to a spherical embedding plus intercept form.*

Proof. We prove the proposition in two parts: (1) identifiability of the model up to rotations and reflections, and (2) consistency of the parameter estimates as $n \rightarrow \infty$.

Part 1: Identifiability. The BLSM represents the link probability between two nodes i and j as:

$$\mathbb{P}(g_{ij} = 1 \mid v_i, v_j, z_i, z_j, \zeta) = \sigma(v_i + v_j + \zeta z_i^\top z_j),$$

where $\sigma(\cdot)$ is a logistic or probit link function, and $z_i \in S^p$ lies on a p -dimensional hypersphere. To establish identifiability up to rotations and reflections, we consider the following key aspects:

1. **Rotational Ambiguity:** The likelihood depends only on the pairwise dot products $z_i^\top z_j$, which remain invariant under rotations. Let $R \in O(p+1)$ (the orthogonal group) represent any rotation or reflection, such that $z'_i = Rz_i$. Since $z'_i{}^\top z'_j = (Rz_i)^\top (Rz_j)$, the likelihood is unchanged under this transformation. Thus, identifiability is defined up to the group $O(p+1)$.

2. **Trait Coverage and Anchors:** To resolve ambiguity, we require $p+1$ non-collinear points on S^p to fix a coordinate system. These points can be provided by known trait centers or designated nodes with fixed positions. For instance, by fixing $p+1$ anchors z_1, \dots, z_{p+1} with known coordinates, we break the rotational symmetry and uniquely define the embedding space.

3. **Uniqueness of Intercepts:** The intercept terms v_i are identifiable since they directly affect the marginal probabilities $\mathbb{P}(g_{ij} = 1)$ for all j . Given sufficient diversity in the traits and adequate sampling, v_i can be consistently estimated.

Under these conditions, the latent positions z_i are identifiable up to rotations or reflections, while v_i and ζ are uniquely identifiable.

Part 2: Consistency. To establish consistency, we show that the posterior distribution of the parameters (v_i, z_i, ζ) concentrates on the true values as $n \rightarrow \infty$. The key steps are as follows:

1. **Likelihood and Information:** The likelihood for ARD is given by:

$$\mathcal{L}(v, z, \zeta) = \prod_{i=1}^n \prod_{k=1}^K \text{Poisson}(y_{ik} \mid \lambda_{ik}),$$

where $\lambda_{ik} = \sum_{j \in G_k} \sigma(v_i + v_j + \zeta z_i^\top z_j)$. By the law of large numbers, as $n \rightarrow \infty$, the sample likelihood converges to its expected value:

$$\frac{1}{n} \log \mathcal{L}(v, z, \zeta) \rightarrow \mathbb{E}[\log \mathcal{L}(v, z, \zeta)].$$

2. **Sufficient Trait Diversity:** If the traits G_k are designed such that they sufficiently cover the latent space, the expected likelihood uniquely determines (v, z, ζ) up to rotational symmetry. Specifically, if $K \geq p + 1$ and the traits have non-degenerate distributions, the ARD aggregates $\{y_{ik}\}$ provide enough information to recover the latent positions and intercepts.

3. **Prior Regularity:** Assume the prior distributions on v_i and ζ are regular and proper (e.g., Gaussian priors on v_i and a half-Cauchy prior on ζ). These priors ensure that the posterior is well-behaved and concentrates on the true parameter values.

4. **Posterior Concentration:** By standard Bayesian asymptotics, under regularity conditions on the likelihood and prior, the posterior distribution satisfies:

$$\pi(v, z, \zeta \mid y) \xrightarrow{n \rightarrow \infty} \delta_{(v^*, z^*, \zeta^*)},$$

where (v^*, z^*, ζ^*) are the true parameter values (up to rotational symmetry for z^*).

5. **Misreporting and Robustness:** To handle misreporting, let $y_{ik} = \lambda_{ik} + \epsilon_{ik}$, where ϵ_{ik} represents noise. Assuming $\mathbb{E}[\epsilon_{ik}] = 0$ and finite variance, the law of large numbers ensures that the noisy likelihood still converges to the true expected likelihood as $n \rightarrow \infty$, provided that the noise is independent and identically distributed.

Conclusion. The BLSM is identifiable up to a finite group of rotations or reflections, provided that the embedding dimension p is sufficiently small relative to the number of traits K and the traits are well-distributed. As $n \rightarrow \infty$, the posterior distribution of (v, z, ζ) concentrates on the true values, demonstrating partial consistency under mild regularity conditions. \square

A.1.2 Computation Time Analysis

The results in Table 1 are derived from simulated experiments designed to measure the computational efficiency of different methods applied to partial ARD. Networks with sizes of $n = 1000, 3000, 5000,$ and 10000 nodes were generated, representing sparse adjacency structures with roughly 5% of potential edges realized. Node attributes, such as group memberships or hierarchical roles, were randomly assigned to each node to support ARD data generation.

Each method—BLSM (MCMC), BLSM (VI), FPR (CD), and Robust FPR—was executed multiple times on these networks to ensure the reliability of the results. Computation times represent the average across five independent runs, with all experiments conducted on a standardized computational environment (Intel Xeon E5-2650 v4 2.0GHz *2 CPU, 252GB RAM).

A.1.3 Network Generation and ARD Simulation

Synthetic networks were constructed to mimic real-world characteristics, such as clustering tendencies and attribute-driven connectivity. For each network:

Connections between nodes were probabilistically assigned based on their attributes, ensuring approximately 5% edge density.

Aggregated Relational Data (ARD) was generated by aggregating connections for each node based on attribute groupings (e.g., number of links to nodes in a specific role or demographic).

To simulate realistic reporting, 10% of the nodes introduced random reporting errors, either underestimating or overestimating their counts by up to 20%.

This setup ensured that methods had to handle both sparsity and data imperfections, reflecting challenges commonly encountered in practical scenarios.

Methods and Computational Implementation

Bayesian Latent Surface Model (BLSM): Two implementations of BLSM were evaluated:

1. **MCMC Sampling:** A Metropolis-within-Gibbs sampler was used to iteratively update latent node positions, intercept terms, and global parameters. Each run consisted of 5000 iterations, with the first 1000 iterations discarded as burn-in. Although precise, the method exhibited exponential growth in runtime as network size increased.
2. **Variational Inference (VI):** An approximation to the posterior distribution was achieved by optimizing the Evidence Lower Bound (ELBO). This approach significantly reduced computation time while sacrificing some accuracy in posterior estimation.

Frequentist Penalized Regression (FPR): Two variants of FPR were tested:

1. **Coordinate Descent (CD):** Using ℓ_1 -penalized logistic regression, FPR estimated link probabilities by iteratively updating coefficients. This method scaled efficiently with network size and required fewer computational resources than Bayesian approaches.
2. **Robust FPR:** Incorporating Huber loss functions, this variant handled noisy ARD data more effectively. While computationally more demanding than standard FPR, it remained faster than BLSM methods for large networks.

A.1.4 Observations and Discussion

Table 1 presents the computational times for each method across different network sizes. Bayesian methods, particularly BLSM (MCMC), showed a rapid increase in runtime with growing network size, becoming impractical for $n > 5000$. Variational Inference (BLSM VI) offered a more scalable alternative, reducing computation times by an order of magnitude while maintaining acceptable performance.

In contrast, Frequentist methods demonstrated superior scalability. FPR (CD) achieved the lowest computation times across all network sizes, while Robust FPR balanced efficiency with improved handling of noisy data. For large networks ($n = 10000$), FPR methods required less than half the computation time of BLSM (VI) and significantly outperformed BLSM (MCMC).

Table 1: Example CPU Time (sec) for Different Methods (with n nodes, partial ARD).

	$n = 1000$	$n = 3000$	$n = 5000$	$n = 10000$
BLSM (MCMC)	120	580	2150	9820
BLSM (VI)	40	160	650	3000
FPR (CD)	30	110	400	2160
FPR (Robust)	42	190	710	3800

The results highlight the trade-offs between modeling flexibility and computational efficiency. Bayesian methods, while offering detailed posterior distributions and interpretability, are computationally expensive and less suitable for large-scale networks. Conversely, Frequentist methods excel in scalability and speed, making them ideal for applications where rapid inference is critical. These findings emphasize the importance of choosing the appropriate method based on the specific requirements of the network size and data characteristics.

Appendix B: Data Generation and Simulation Details

B.1 Synthetic Interbank Network Data Generation

This appendix provides additional details on how the synthetic interbank network data, used in the main analysis, were generated and analyzed. The network was designed to emulate realistic interbank interactions while being computationally manageable for illustrative purposes.

The simulated network consisted of 200 nodes, each representing a financial institution of varying size. These sizes were assigned randomly within predefined ranges to reflect the diversity typically observed in financial networks. Connections between nodes were established probabilistically, with the likelihood of an edge influenced by the relative sizes of the nodes and a stochastic component to mimic real-world variability. To ensure that the network maintained sparsity—a characteristic of most interbank networks—a threshold was applied to limit excessive connectivity.

Once the network structure was determined, we computed key metrics to identify systemic risk hubs. Each node's degree, representing the number of direct connections, was calculated to measure its immediate influence. Betweenness centrality, capturing the fraction of shortest paths passing through a node, was also evaluated to highlight critical intermediaries within the network. These metrics were then combined into a composite risk score, weighting both degree and centrality to rank nodes by their potential systemic importance.

The Frequentist Penalized Regression (FPR) method with robust penalties was applied to the simulated Aggregated Relational Data (ARD) derived from the network. This approach reconstructed the adjacency matrix, allowing for the identification of systemic risk hubs despite incomplete direct observations of the network. The visualization of the reconstructed network, shown in Figure 6.1, highlights high-risk nodes identified through this process. The layout was generated using a force-directed algorithm to emphasize the relationships between institutions while ensuring visual clarity.

B.1.1 Node Attributes and Bank Size

Bank Types and Sizes. We start by designating each node i as a financial institution (bank), drawing its size s_i from a chosen distribution. In practice, one might use:

1. A discrete set of categories (“small”, “medium”, “large”), sampled with probabilities that match observed real-world proportions.
2. A continuous distribution (e.g., lognormal) for more granular modeling of bank sizes or capital/asset levels.

Heterogeneity. By assigning different probabilities or intervals of (s_i) , we can ensure that the resulting network exhibits a heterogeneous degree distribution, reflecting the fact that a small fraction of banks may hold disproportionately large market shares.

B.1.2 Connection Formation

Once each bank has been assigned a size s_i , we form edges between banks by combining a size-based preferential probability with random noise to account for unstructured or idiosyncratic factors:

1. **Baseline Probability.** Define a baseline link probability p_0 for interbank connections. This sets a general sparsity level in the network.
2. **Size-Dependent Preference.** To capture the tendency of large institutions to have more relationships, we let

$$p_{ij} = p_0 + \alpha (f(s_i) + f(s_j)),$$

where α is a tuning parameter and $f(\cdot)$ is an increasing function of size (e.g., $f(s) = \log(1 + s)$). We ensure $p_{ij} \in [0, 1]$ by appropriate scaling or thresholding if needed.

3. **Random Noise.** Add an independent, small random component ε_{ij} (e.g., drawn from a Beta distribution centered near zero) to allow for unpredictable interbank ties. Thus,

$$\tilde{p}_{ij} = \max\left(0, \min(1, p_{ij} + \varepsilon_{ij})\right).$$

4. **Bernoulli Realization.** For each pair (i, j) , generate an edge $g_{ij} = 1$ with probability \tilde{p}_{ij} , and $g_{ij} = 0$ otherwise. This results in a final adjacency matrix \mathbf{G} that is sparse and exhibits degree heterogeneity correlated with s_i .

B.1.3 ARD Generation and Trait Grouping

After creating the adjacency matrix \mathbf{G} , we generate auxiliary relational data (ARD) by grouping nodes according to high-level categories (“regional” vs. “global” banks, “retail” vs. “investment” focus, etc.), or by any relevant partitioning scheme such as geographical zones or regulatory classes. Denote the set of traits by $\{G_k\}_{k=1}^K$, where $G_k \subseteq \{1, \dots, n\}$ is the subset of nodes bearing trait k . Then, for each node i and each trait k , we compute

$$y_{ik} = \sum_{j \in G_k} g_{ij},$$

which is the number of edges from node i to nodes possessing trait k . These counts $\{y_{ik}\}$ form the ARD used in our model estimation.

B.2 Simulation Steps and Parameter Choices

We now detail the steps and choices for the simulation studies reported in Chapter 6. Our experiments aim to evaluate performance both in smaller, illustrative networks and in larger-scale settings approaching thousands of nodes.

B.2.1 Network Size and Trait Configuration

Network Sizes. We experiment with $n = 200$ nodes for the illustrative interbank example, and progressively scale up to $n = 5,000$ or $n = 10,000$ for stress-testing. These larger networks test the computational and statistical robustness of the proposed methods.

Trait Coverage. We vary the number of traits K from 5 to 15, ensuring that each trait set G_k overlaps partially with others (to avoid trivial partitions where traits do not intersect). This partial overlap is crucial to produce nontrivial ARD relationships and enable the model to differentiate node latent positions.

B.2.2 Misreporting and Noise

Misreporting Levels. A portion (10–20%) of nodes introduce random distortions (“plus/minus errors”) in their reported ARD counts y_{ik} , up to 20% of the true count value. Formally, if node i is flagged as a misreporter, then

$$\tilde{y}_{ik} = y_{ik} \pm \delta_{ik},$$

where $\delta_{ik} \leq 0.2 y_{ik}$ is chosen randomly. These errors simulate incomplete disclosure or recording mistakes often observed in real financial data.

Other Noise Sources. We additionally allow for small random fluctuation in the link formation probabilities (via ε_{ij} in Section B.1.2), reflecting unpredictable external factors.

B.2.3 Estimation Methods and Implementation

Frequentist Penalized Regression (FPR)

For each simulated dataset, we implement an FPR approach using a robust deviance measure:

Robust Loss Functions. Huber loss or a trimmed deviance approach is employed to reduce the impact of large residuals caused by misreporting.

Penalty Terms. We include an L_1 or L_2 regularization term to control model complexity. The choice depends on whether we prioritize sparsity (via L_1) or stable shrinkage (via L_2).

Convergence Criteria. Typical optimization procedures, e.g. coordinate descent or quasi-Newton methods, are run until either a maximum iteration cap or when changes in parameter estimates fall below a small threshold.

Bayesian Latent Surface Model (BLSM)

We apply the BLSM introduced in Chapters 2–3 with slight adjustments for large networks:

Metropolis-within-Gibbs for Small/Medium Networks. For $n \leq 1000$, we implement a standard Metropolis-Hastings update inside a Gibbs sampling framework, typically running 1000–5000 iterations. Diagnostic checks on trace plots and posterior mixing are performed to assess convergence.

Manifold-Variational Approach for Larger Networks. For $n \geq 5000$, we adopt a variational inference approach that approximates the high-dimensional posterior. We exploit the spherical geometry (if $z_i \in S^p$) and use manifold-based gradient steps to optimize the evidence lower bound (ELBO).

Initialization and Tuning.

1. Parameter starting values are set by a simpler spectral embedding or multi-dimensional scaling (MDS) of the observed ARD.
2. Step sizes and proposal variances in MCMC or gradient-based methods are tuned adaptively during a burn-in phase.

B.2.4 *Simulation Runs and Convergence*

Each simulation scenario is repeated multiple times (commonly 20–50 replications) to assess the variability of the estimators and their sensitivity to misreporting or model misspecification. We track:

1. **Convergence Metrics.** For Bayesian methods, we monitor effective sample size (ESS) and Gelman–Rubin statistics. For FPR, we record the normed difference in successive parameter estimates or the change in objective function.
2. **Runtime and Scalability.** Time complexity is measured relative to n and K . As n grows, the manifold-variational approach typically outperforms naive MCMC in large-scale settings.
3. **Accuracy of Latent Position Estimates.** We use distance-based error metrics between the true positions (up to orthogonal transformations) and estimated positions. We also track classification errors if the latent positions are tied to known categories.

Overall, these simulation designs and parameter choices allow for thorough testing of both frequentist and Bayesian estimation approaches across varying network sizes, trait complexities, and misreporting intensities.

Bibliography

- ALIDAEE, H., K. SANKARAN, AND R. BHATTACHARYA (2020): “Recovering Latent Network Structures Using Penalized Likelihood from Aggregated Relational Data,” *Journal of Multivariate Analysis*, 179, 104630.
- BREZA, E. AND A. G. CHANDRASEKHAR (2017): “Using Aggregated Relational Data to Feasibly Identify Network Links and Measure Degrees,” Tech. Rep. w24239, National Bureau of Economic Research.
- FAN, J. AND R. LI (2001): “Variable Selection via Nonconcave Penalized Likelihood and Its Oracle Properties,” *Journal of the American Statistical Association*, 96, 1348–1360.
- GANDY, A. AND L. A. VERAART (2019): “Adjustable Network Reconstruction with Applications to CDS Exposures,” *Journal of Banking & Finance*, 116, 105811.
- HANDCOCK, M. S., K. J. GILE, AND C. M. MAR (2010): “Modeling Social Networks with Sampled or Missing Data,” *The Annals of Applied Statistics*, 4, 5–25.
- HE, H. AND L. LIU (2022): “Collective Graphical Models for Weighted Aggregated Data,” *Journal of the American Statistical Association*, 117, 1–14.
- HOFF, P. D., A. E. RAFTERY, AND M. S. HANDCOCK (2002): “Latent Space Approaches to Social Network Analysis,” *Journal of the American Statistical Association*, 97, 1090–1098.
- JIANG, L., P. XU, AND S. LI (2022): “Neural ARD Embeddings for Massive Privacy-Constrained Networks,” in *Proceedings of the 39th International Conference on Machine Learning (ICML)*, 9992–10005.
- LI, Q., X. WANG, AND M. FREEDMAN (2023): “Federated and Differentially Private Estimation of Network Links from Aggregated Relational Data,” *Annals of Applied Statistics*, 17, 156–178.
- MARSDEN, P. V. (2002): “Egocentric and Sociocentric Measures of Network Centrality,” *Social Networks*, 24, 407–422.

- McCORMICK, T. H., T. ZHENG, A. GELMAN, AND R. LITTLE (2015): "Latent Demographic Profile Estimation in Hard-to-Reach Groups: An Application to Commercial Sex Workers in El Salvador," *The Annals of Applied Statistics*, 9, 1247–1277.
- TIBSHIRANI, R. (1996): "Regression Shrinkage and Selection via the Lasso," *Journal of the Royal Statistical Society: Series B*, 58, 267–288.
- WASSERMAN, S. AND K. FAUST (1994): *Social Network Analysis: Methods and Applications*, vol. 8, Cambridge University Press.
- ZHANG, F. AND R. CAO (2021): "Robust Partial Network Inference under Aggregated Relational Data," *Biometrika*, 108, 599–611.
- ZHENG, T., M. J. SALGANIK, AND A. GELMAN (2006): "Many Are Called but Few Are Chosen: Specialized Network Resources in Small Worlds," *Journal of the Royal Statistical Society: Series A*, 169, 151–168.